A three-step inversion method based on compressive sensing for imaging sparse scatterers

L. Poli, G. Oliveri, F. Viani, A. Massa

Abstract

This report is aimed at validating an innovative and efficient procedure, still within the CSI probabilistic framework, able to reliably retrieve sparse complex current coefficients by enforcing the interrelationships between their real and imaginary components exploiting a multi-task approach. Towards this end, a set of numerical experiments are proposed, comparing the performance of the multi-task approach with the standard single-task version with uncorrelated coefficients associated to the real and imaginary part of the currents.

1 Legend

- ST-BCS is the single-task Bayesian Compressive Sampling-based technique.
- MT-BCS-Jmn is the multi-task Bayesian Compressive Sampling-based technique that exploits the correlation between the real and imaginary parts of the source.

2 Calibration

2.1 TEST CASE: Square Cylinder $L = 0.16\lambda$

Goal: show the performances of BCS when dealing with a sparse scatterer

- Number of Views: V
- Number of Measurements: M
- Number of Cells for the Inversion: N
- Number of Cells for the Direct solver: D
- Side of the investigation domain: L

Test Case Description

Direct solver:

- Square domain divided in $\sqrt{D} \times \sqrt{D}$ cells
- Domain side: $L = 3\lambda$
- $D = 1296$ (discretization for the direct solver: $< \lambda/10$)

Investigation domain:

- Square domain divided in $\sqrt{N} \times \sqrt{N}$ cells
- $L = 3\lambda$
- $2ka = 2 \times \frac{2\pi}{\lambda} \times \frac{L\sqrt{2}}{2} = 6\pi\sqrt{2} = 26.65$
- $\#DOF = \frac{(2ka)^2}{2} = \frac{(2 \times \frac{2\pi}{\lambda} \times \frac{L\sqrt{2}}{2})^2}{2} = 4\pi^2 \left(\frac{L}{\lambda}\right)^2 = 4\pi^2 \times 9 \approx 355.3$
- N scelto in modo da essere vicino a $\#DOF$: $N = 324$ (18×18)

Measurement domain:

- Measurement points taken on a circle of radius $\rho = 3\lambda$
- Full-aspect measurements
- $M \approx 2ka \rightarrow M = 27$

Sources:

- Plane waves
- $V \approx 2ka \rightarrow V = 27$
- Amplitude: $A = 1$
- Frequency: 300 MHz $(\lambda = 1)$

Object:

- Square cylinder of side $\frac{\lambda}{6} = 0.1667$
- $\varepsilon_r = 2.0$
- $\sigma = 0$ [S/m]

BCS parameters:

- Gamma prior on noise variance parameter: $a \in \left\{1 \times 10^{0}, 2 \times 10^{0}, 5 \times 10^{0},\ 1 \times 10^{+1}, 2 \times 10^{+1}, 5 \times 10^{+1}, 1 \times 10^{+2}, 2 \times 10^{+2}, 5 \times 10^{+2}, 1 \times 10^{+3}, 2 \times 10^{+3}, 5 \times 10^{+3}, 1 \times 10^{+4}\right\}$
- Gamma prior on noise variance parameter: $b \in \left\{1 \times 10^{+0}, 5 \times 10^{-1}, 2 \times 10^{-1}, 1 \times 10^{-1}, 5 \times 10^{-2}, 2 \times 10^{-2}\ 1 \times 10^{-2}, 5 \times 10^{-3}, 2 \times 10^{-3}, 1 \times 10^{-3}, 5 \times 10^{-4}, 2 \times 10^{-4}, 1 \times 10^{-4}\right\}$
- Convergenze parameter: $\tau = 1.0 \times 10^{-8}$

RESULTS: Calibration

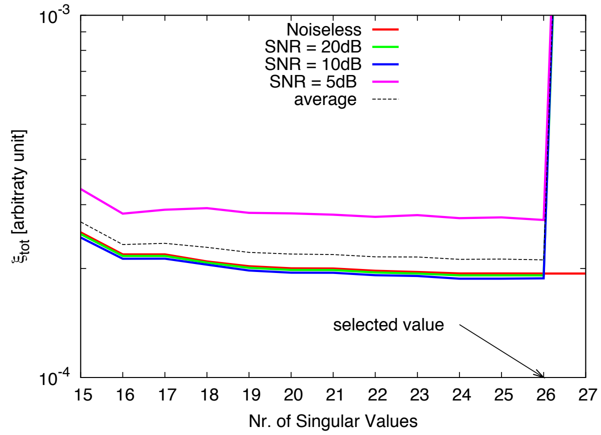

(a)

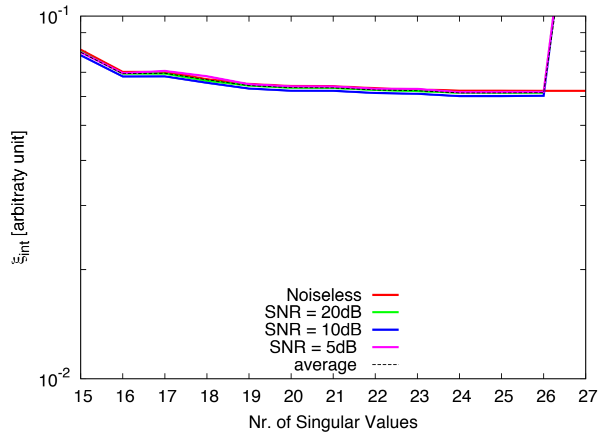

(b)

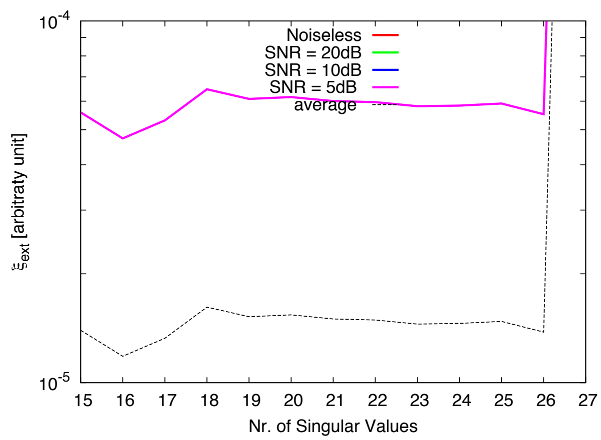

(c)

Figure 1. Behaviour of error figures as a function of the initial estimate of the noise n_0, for different SNR values: (a) total error ξ_{tot}, (b) internal error ξ_{int}, (c) external error ξ_{ext}.

Obervations:

The error function ξ_{tot} (averaged considering different SNR values: Noiseless, $SNR = 20dB$, $SNR = 10dB$ and $SNR = 5dB$) depending on the parameters (a, b) has a global minimum in $(a = 5 \times 10^0$, $b = 8 \times 10^{-2})$

indipendently from the number of Singular Values selected. However, the depth of the global minimum depends on the number of Singular Values, Fig. 1 shows the values of the global minimum of the averaged error function ξ_{tot} with respect to the number of Singular Values. We have the deepest global minimum for 26 singular values.

RESULTS: Calibration - Nr. of Singular Values: $\rho = 26$

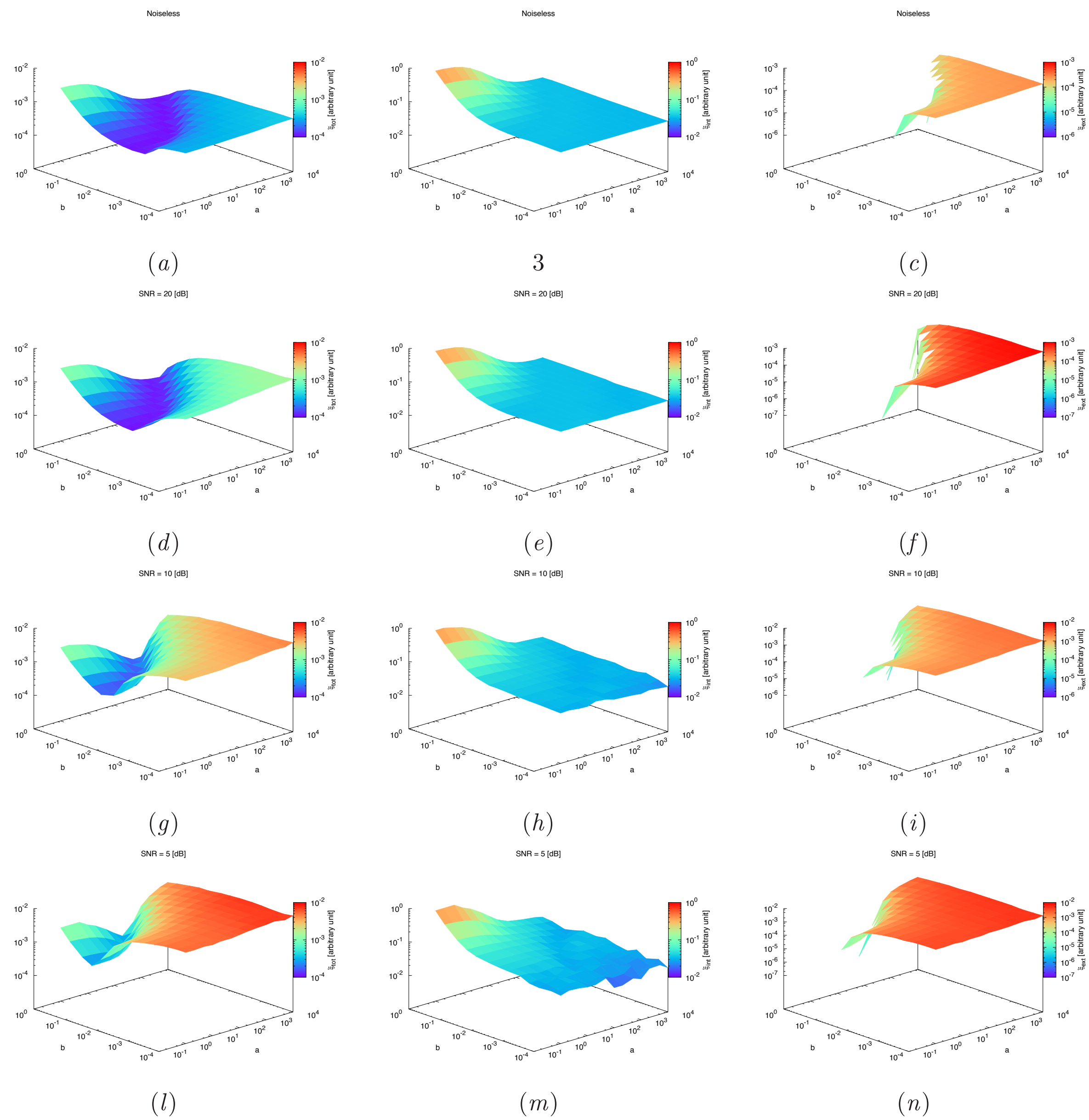

Figure 2. Behaviour of error figures as a function of the initial estimate of the Gamma prior on the noise variance parameters a and b, for different SNR values: (a), (d), (g) and (l) total error ξ_{tot}, (b), (e), (h) and (m) internal error ξ_{int}, (c), (f), (i) and (n) external error ξ_{ext}, for (a), (b) and (c) Noiseless case, (d), (e) and (f) $SNR = 20dB$, (g), (h) and (i) $SNR = 10dB$ and (l), (m) and (n) $SNR = 5dB$.

RESULTS: Calibration - Nr. of Singular Values: $\rho = 26$

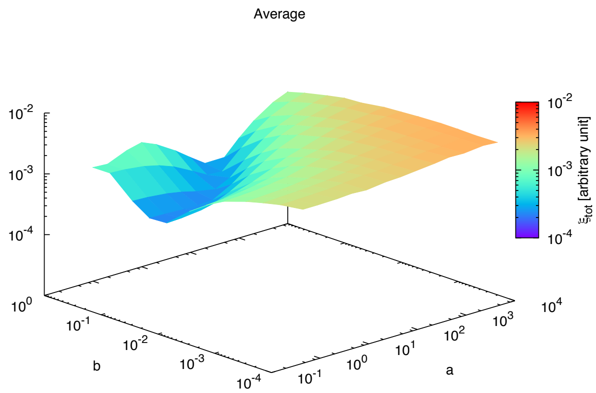

(a)

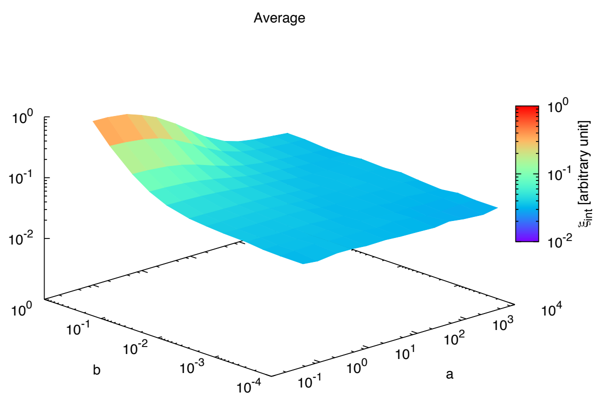

(b)

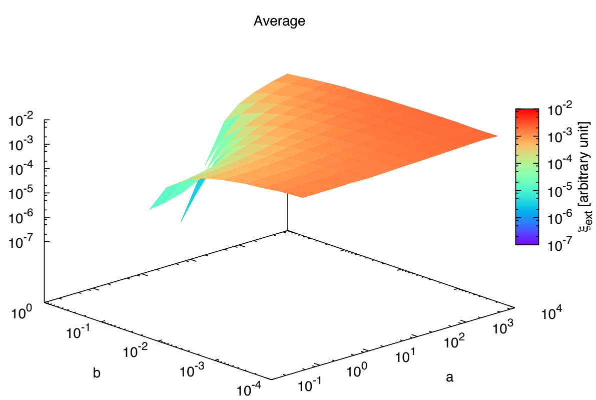

(c)

Figure 3. Averaged behaviour of error figures as a function of the initial estimate of the Gamma prior on the noise variance parameters a and b: (a) total error ξ_{tot}, (b) internal error ξ_{int}, (c) external error ξ_{ext}.

3 Tests Dominio $L = 3.00\lambda$

3.1 TEST CASE: Cross-Shaped Cylinder

Goal: show the performances of BCS when dealing with a sparse scatterer

- Number of Views: V
- Number of Measurements: M
- Number of Cells for the Inversion: N
- Number of Cells for the Direct solver: D
- Side of the investigation domain: L

Test Case Description

Direct solver:

- Square domain divided in $\sqrt{D} \times \sqrt{D}$ cells
- Domain side: $L = 3\lambda$
- $D = 1296$ (discretization for the direct solver: $< \lambda/10$)

Investigation domain:

- Square domain divided in $\sqrt{N} \times \sqrt{N}$ cells
- $L = 3\lambda$
- $2ka = 2 \times \frac{2\pi}{\lambda} \times \frac{L\sqrt{2}}{2} = 6\pi\sqrt{2} = 26.65$
- $\#DOF = \frac{(2ka)^2}{2} = \frac{(2\times\frac{2\pi}{\lambda}\times\frac{L\sqrt{2}}{2})^2}{2} = 4\pi^2\left(\frac{L}{\lambda}\right)^2 = 4\pi^2 \times 9 \approx 355.3$
- N scelto in modo da essere vicino a $\#DOF$: $N = 324$ (18×18)

Measurement domain:

- Measurement points taken on a circle of radius $\rho = 3\lambda$
- Full-aspect measurements
- $M \approx 2ka \rightarrow M = 27$

Sources:

- Plane waves
- $V \approx 2ka \rightarrow V = 27$
- Amplitude: $A = 1$
- Frequency: 300 MHz ($\lambda = 1$)

Object:

- Cross-shaped cylinder
- $\varepsilon_r \in \{1.5, 2.0, 2.5, 3.0, 3.5, 4.0, 4.5, 5.0\}$
- $\sigma = 0$ [S/m]

MT-BCS-Jmn parameters:

- Gamma prior on noise variance parameter: $a = 5 \times 10^0$
- Gamma prior on noise variance parameter: $b = 8 \times 10^{-2}$
- Convergenze parameter: $\tau = 1.0 \times 10^{-8}$

RESULTS: Cross-Shaped Cylinder

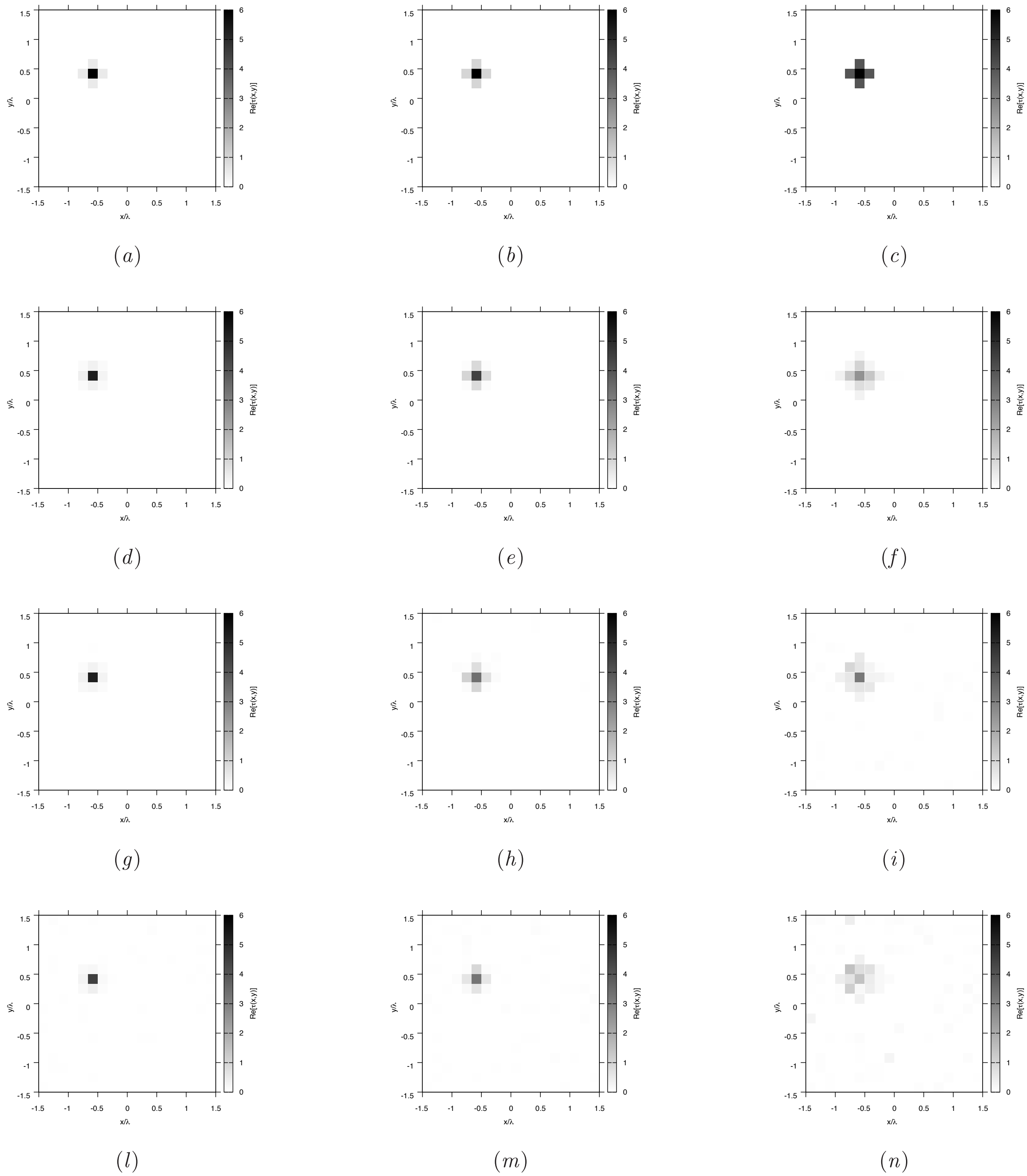

Figure 10. Actual object $(a)(b)(c)$ and MT-BCS-Jmn reconstructed object with $\varepsilon_r = 1.5$ $(d)(g)(l)$, $\varepsilon_r = 2.0$ $(e)(h)(m)$, and $\varepsilon_r = 5.0$ $(f)(i)(n)$, for Noiseless case $(d)(e)(f)$, $SNR = 10$ [dB] $(g)(h)(i)$ and $SNR = 5$ [dB] $(l)(m)(n)$.

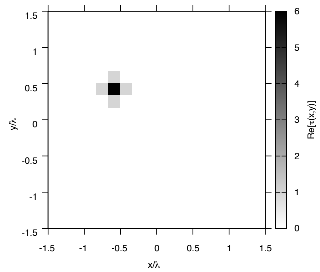

(a)

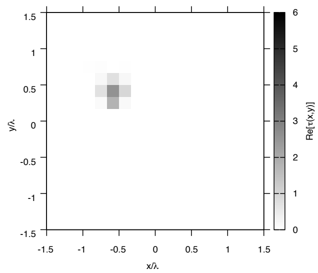

(b)

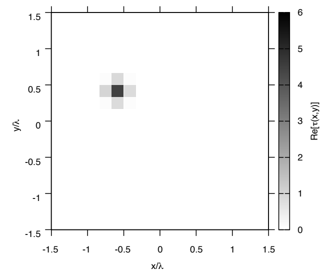

(e)

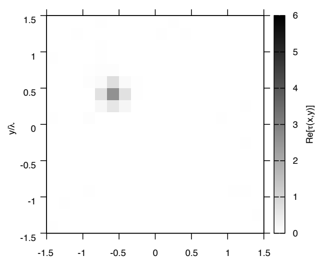

(c)

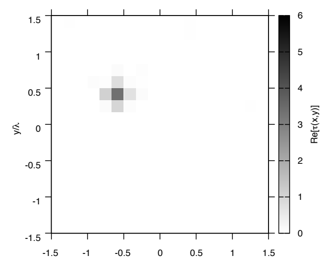

(f)

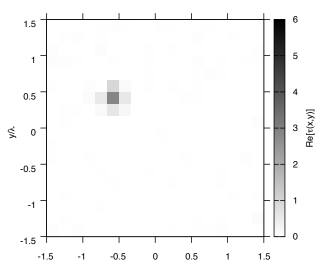

(d)

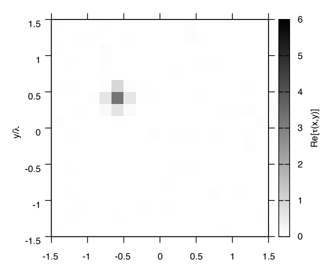

(g)

Figure 11. Actual object (a), ST-BCS reconstructed object $(b)(c)(d)$ and MT-BCS-Jmn reconstructed object $(e)(f)(g)$ for Noiseless case $(b)(e)$, $SNR = 10$ [dB] $(c)(f)$ and $SNR = 5$ [dB] $(d)(g)$.

RESULTS: Cross-Shaped Cylinder - Error Figures - Comparison ST-BCS/MT-BCS

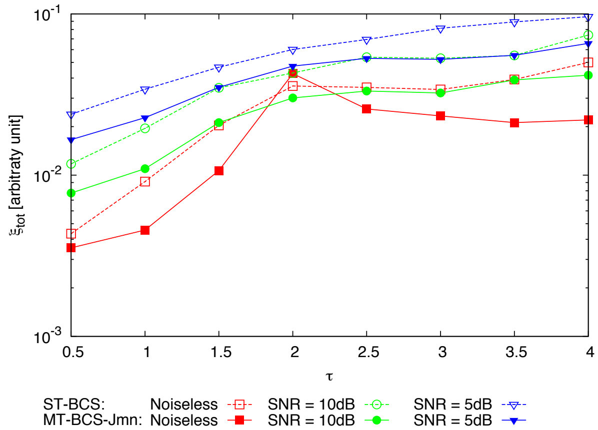

(a)

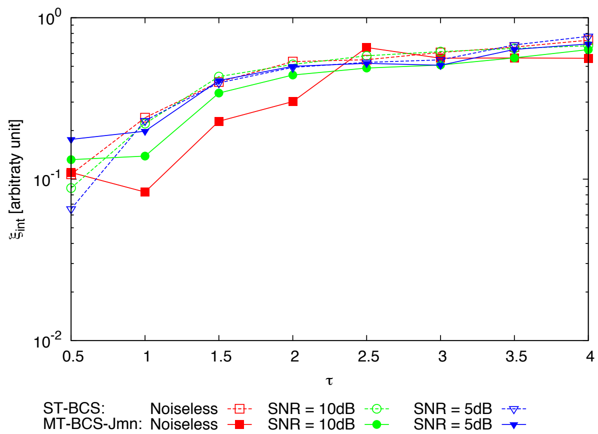

(b)

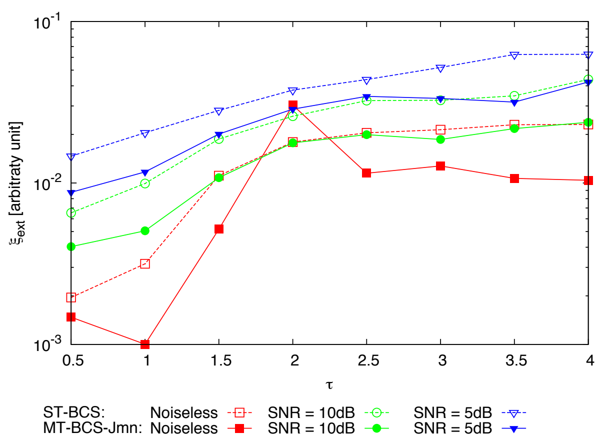

(c)

Figure 12. Behaviour of error figures as a function of ε_r, for different SNR values: (a) total error ξ_{tot}, (b) internal error ξ_{int}, (c) external error ξ_{ext}.

3.2 TEST CASE: L-Shaped Cylinder

Goal: show the performances of BCS when dealing with a sparse scatterer

- Number of Views: V
- Number of Measurements: M
- Number of Cells for the Inversion: N
- Number of Cells for the Direct solver: D
- Side of the investigation domain: L

Test Case Description

Direct solver:

- Square domain divided in $\sqrt{D} \times \sqrt{D}$ cells
- Domain side: $L = 3\lambda$
- $D = 1296$ (discretization for the direct solver: $< \lambda/10$)

Investigation domain:

- Square domain divided in $\sqrt{N} \times \sqrt{N}$ cells
- $L = 3\lambda$
- $2ka = 2 \times \frac{2\pi}{\lambda} \times \frac{L\sqrt{2}}{2} = 6\pi\sqrt{2} = 26.65$
- $\#DOF = \frac{(2ka)^2}{2} = \frac{(2\times\frac{2\pi}{\lambda}\times\frac{L\sqrt{2}}{2})^2}{2} = 4\pi^2\left(\frac{L}{\lambda}\right)^2 = 4\pi^2 \times 9 \approx 355.3$
- N scelto in modo da essere vicino a $\#DOF$: $N = 324$ (18×18)

Measurement domain:

- Measurement points taken on a circle of radius $\rho = 3\lambda$
- Full-aspect measurements
- $M \approx 2ka \rightarrow M = 27$

Sources:

- Plane waves
- $V \approx 2ka \rightarrow V = 27$
- Amplitude $A = 1$
- Frequency: 300 MHz ($\lambda = 1$)

Object:

- L-shaped cylinder
- $\varepsilon_r \in \{1.5, 2.0, 2.5, 3.0, 3.5, 4.0, 4.5, 5.0\}$
- $\sigma = 0$ [S/m]

MT-BCS-Jmn parameters:

- Gamma prior on noise variance parameter: $a = 5 \times 10^0$
- Gamma prior on noise variance parameter: $b = 8 \times 10^{-2}$
- Convergenze parameter: $\tau = 1.0 \times 10^{-8}$

RESULTS: L-Shaped Cylinder

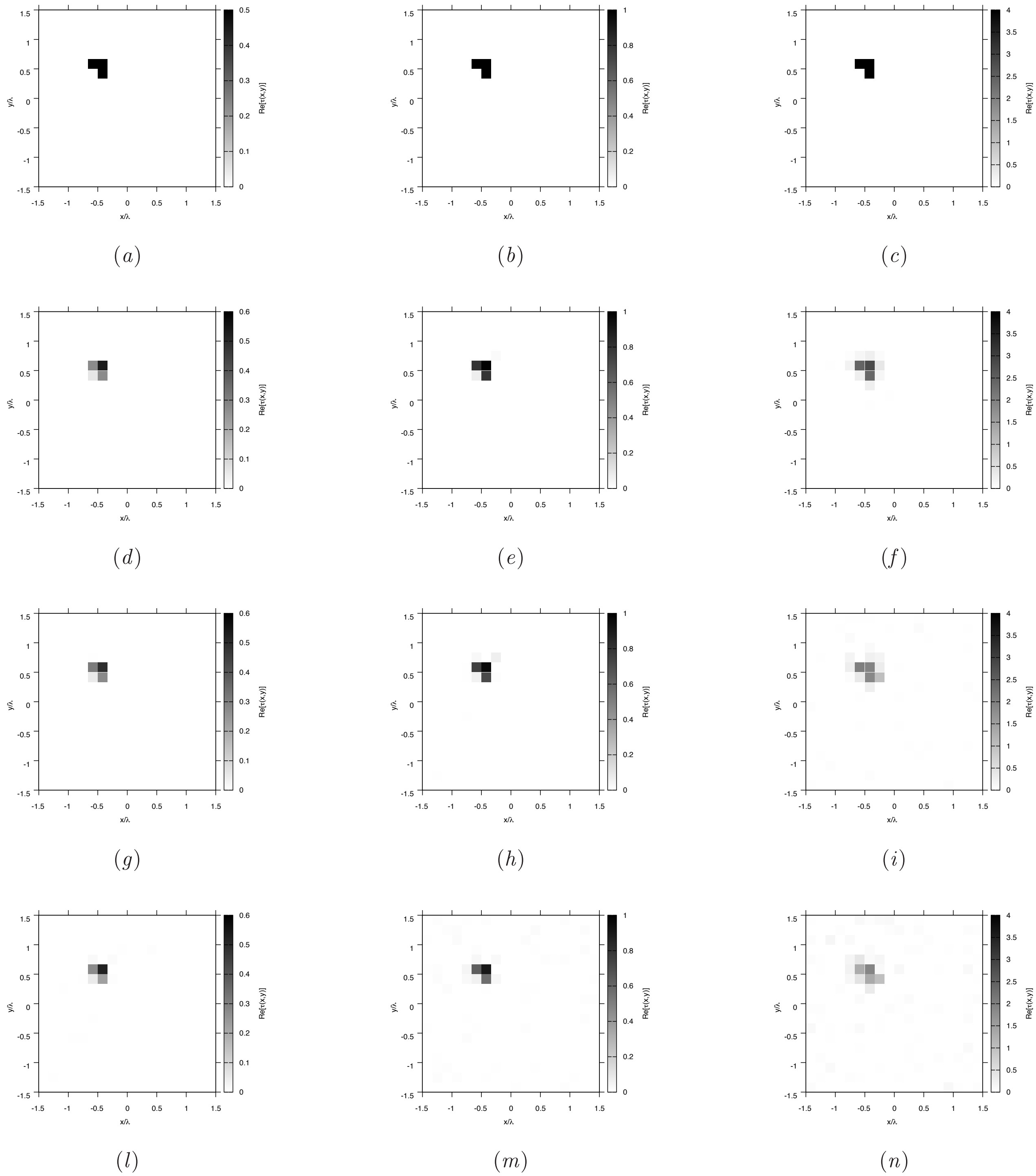

Figure 13. Actual object $(a)(b)(c)$ and MT-BCS-Jmn reconstructed object with $\varepsilon_r = 1.5$ $(d)(g)(l)$, $\varepsilon_r = 2.0$ $(e)(h)(m)$, and $\varepsilon_r = 5.0$ $(f)(i)(n)$, for Noiseless case $(d)(e)(f)$, $SNR = 10$ [dB] $(g)(h)(i)$ and $SNR = 5$ [dB] $(l)(m)(n)$.

RESULTS: L-Shaped Cylinder - Reconstructions - Comparison ST-BCS/MT-BCS - $\varepsilon_r = 2.0$

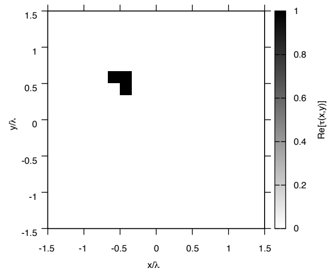

(a)

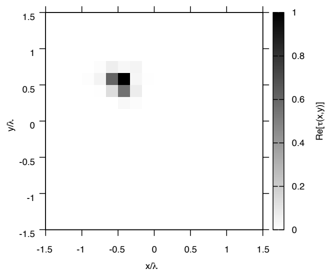

(b)

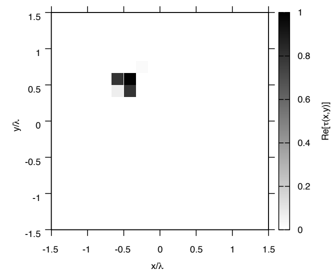

(e)

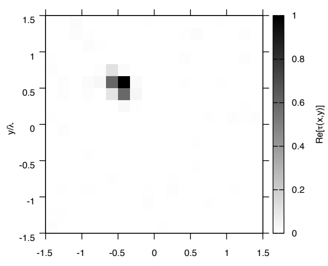

(c)

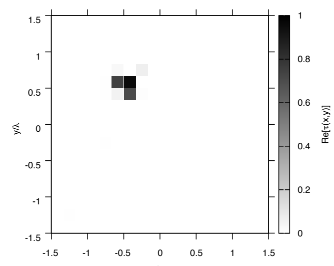

(f)

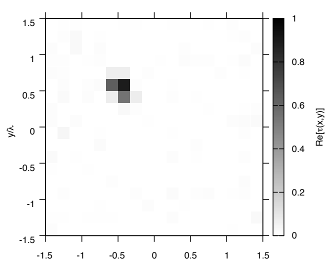

(d)

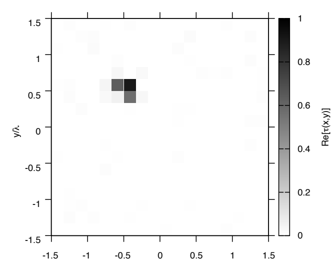

(g)

Figure 14. Actual object (a), ST-BCS reconstructed object $(b)(c)(d)$ and MT-BCS-Jmn reconstructed object $(e)(f)(g)$ for Noiseless case $(b)(e)$, $SNR = 10$ [dB] $(c)(f)$ and $SNR = 5$ [dB] $(d)(g)$.

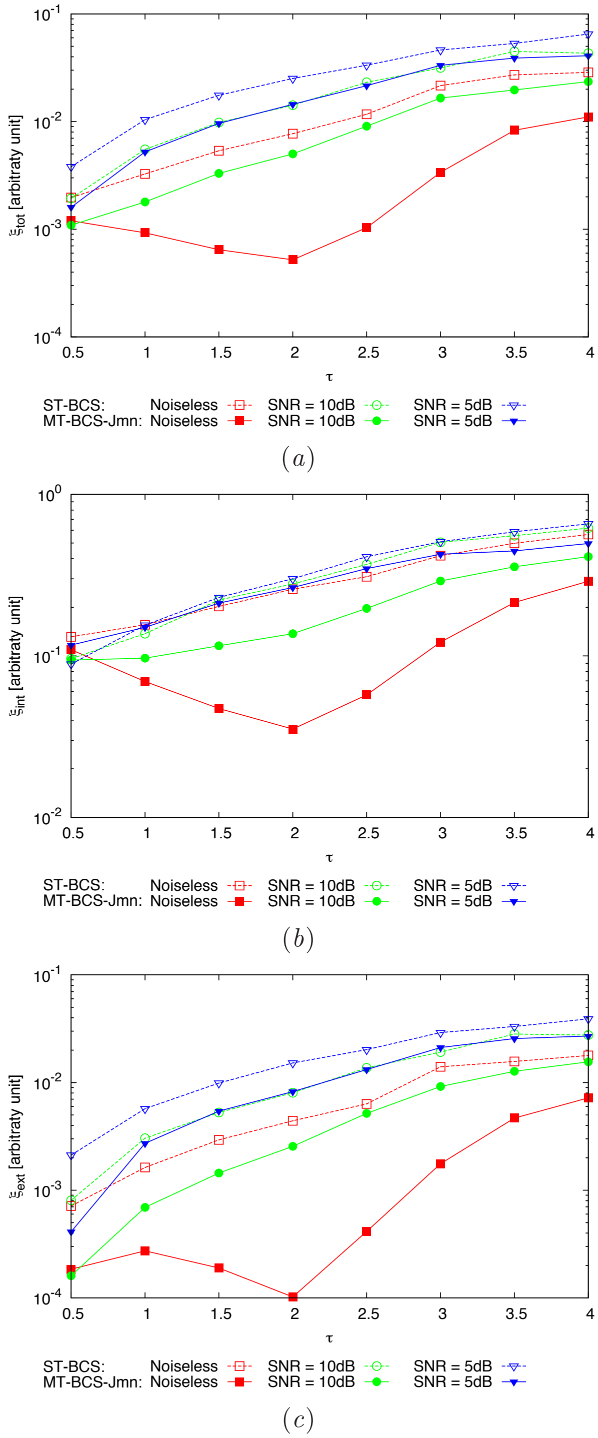

Figure 15. Behaviour of error figures as a function of ε_r, for different SNR values: (a) total error ξ_{tot}, (b) internal error ξ_{int}, (c) external error ξ_{ext}.

3.3 TEST CASE: Inhomogeneous L-Shaped Cylinder

Goal: show the performances of BCS when dealing with a sparse scatterer

- Number of Views: V
- Number of Measurements: M
- Number of Cells for the Inversion: N
- Number of Cells for the Direct solver: D
- Side of the investigation domain: L

Test Case Description

Direct solver:

- Square domain divided in $\sqrt{D} \times \sqrt{D}$ cells
- Domain side: $L = 3\lambda$
- $D = 1296$ (discretization for the direct solver: $< \lambda/10$)

Investigation domain:

- Square domain divided in $\sqrt{N} \times \sqrt{N}$ cells
- $L = 3\lambda$
- $2ka = 2 \times \frac{2\pi}{\lambda} \times \frac{L\sqrt{2}}{2} = 6\pi\sqrt{2} = 26.65$
- $\#DOF = \frac{(2ka)^2}{2} = \frac{(2\times\frac{2\pi}{\lambda}\times\frac{L\sqrt{2}}{2})^2}{2} = 4\pi^2\left(\frac{L}{\lambda}\right)^2 = 4\pi^2 \times 9 \approx 355.3$
- N scelto in modo da essere vicino a $\#DOF$: $N = 324$ (18×18)

Measurement domain:

- Measurement points taken on a circle of radius $\rho = 3\lambda$
- Full-aspect measurements
- $M \approx 2ka \rightarrow M = 27$

Sources:

- Plane waves
- $V \approx 2ka \rightarrow V = 27$
- Amplitude $A = 1$
- Frequency: 300 MHz ($\lambda = 1$)

Object:

- Inhomogeneous L-shaped cylinder
- $\varepsilon_r \in \{1.5, 2.0, 2.5, 3.0, 3.5, 4.0, 4.5, 5.0\}$
- $\sigma = 0$ [S/m]

MT-BCS-Jmn parameters:

- Gamma prior on noise variance parameter: $a = 5 \times 10^0$
- Gamma prior on noise variance parameter: $b = 8 \times 10^{-2}$
- Convergenze parameter: $\tau = 1.0 \times 10^{-8}$

RESULTS: Inhomogeneous L-Shaped Cylinder

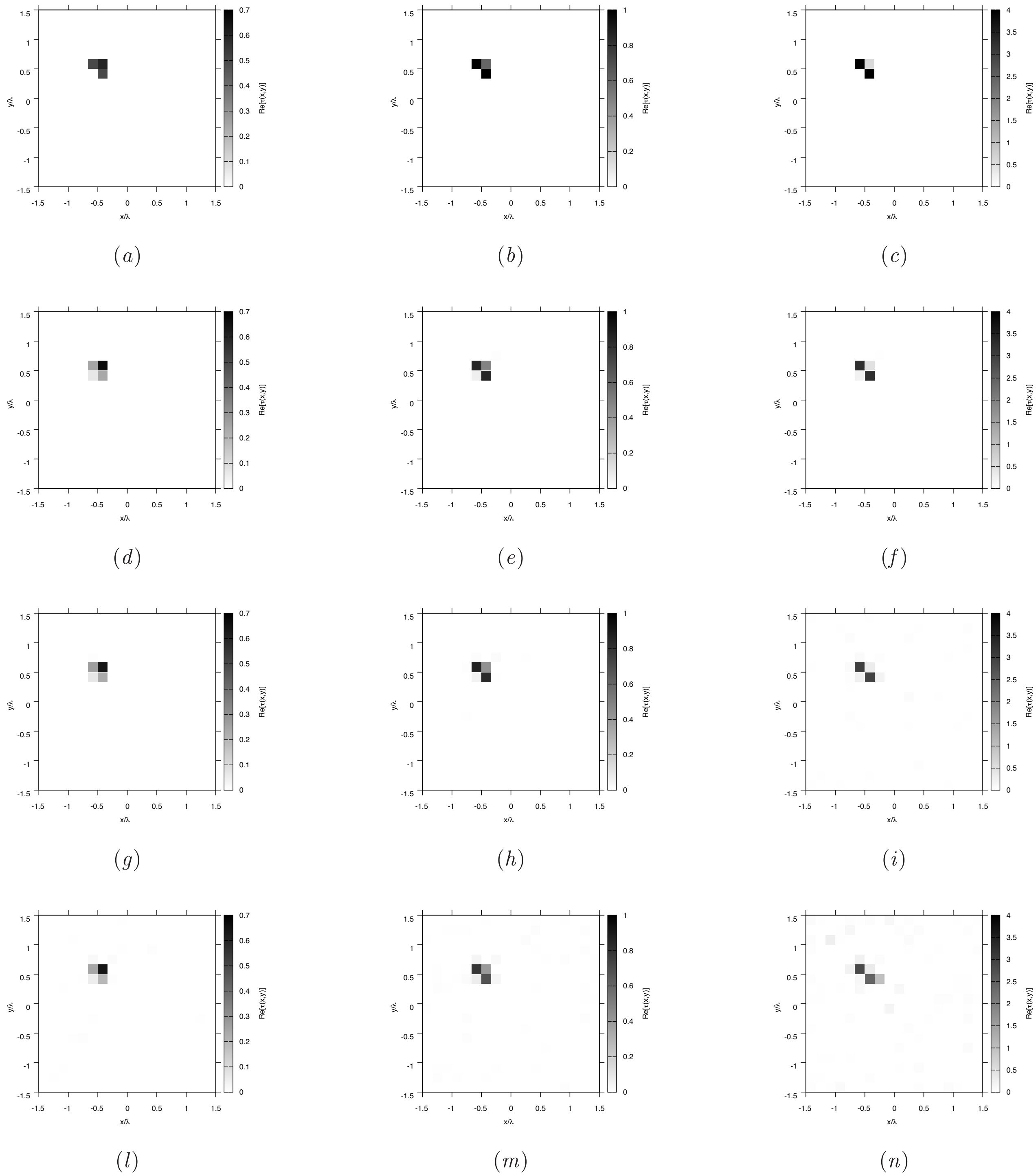

Figure 16. Actual object $(a)(b)(c)$ and MT-BCS-Jmn reconstructed object with $\varepsilon_r = 1.5$ $(d)(g)(l)$, $\varepsilon_r = 2.0$ $(e)(h)(m)$, and $\varepsilon_r = 5.0$ $(f)(i)(n)$, for Noiseless case $(d)(e)(f)$, $SNR = 10$ [dB] $(g)(h)(i)$ and $SNR = 5$ [dB] $(l)(m)(n)$.

RESULTS: Inhomogeneous L-Shaped Cylinder - Reconstructions - Comparison ST-BCS/MT-BCS - $\varepsilon_r = 2.0$

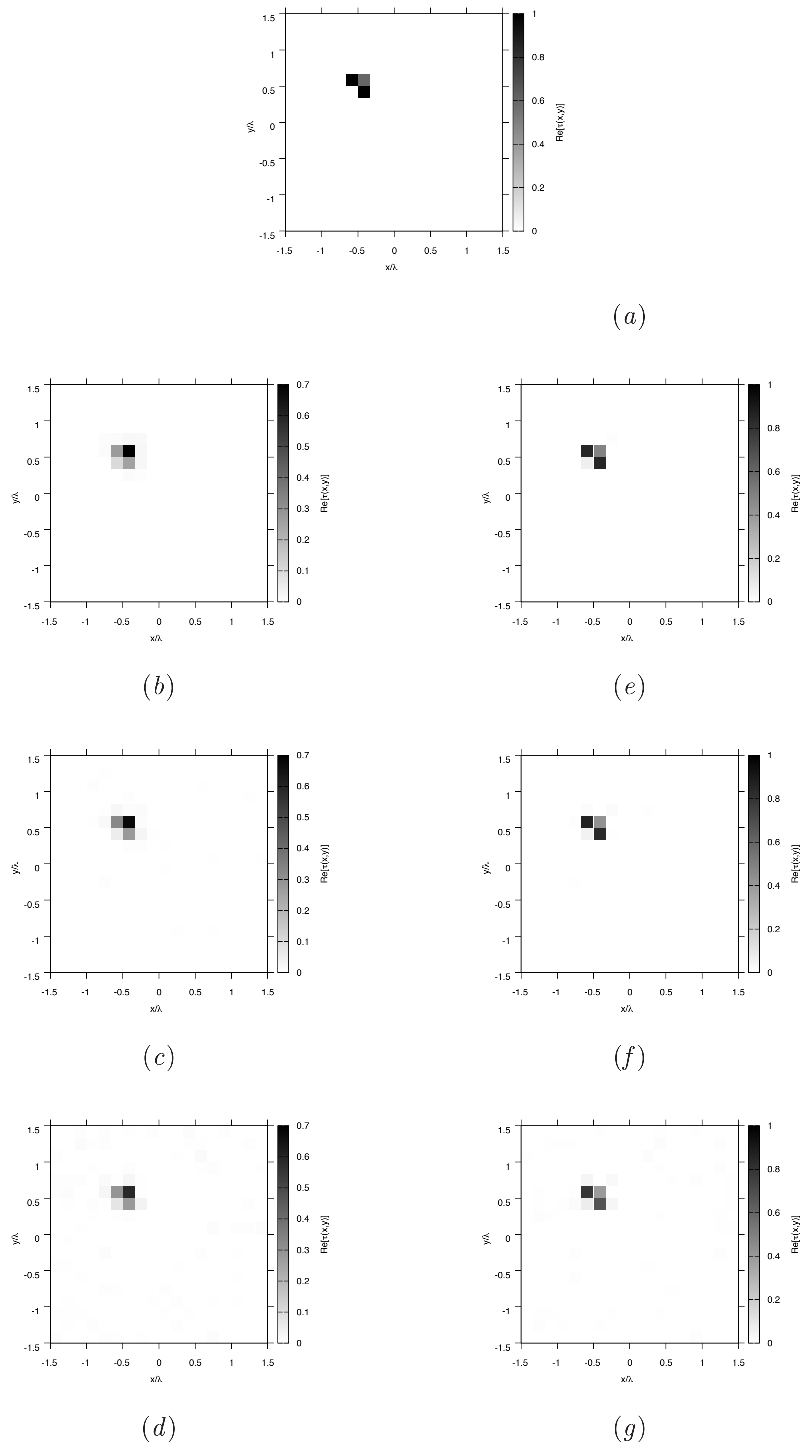

Figure 17. Actual object (a), ST-BCS reconstructed object $(b)(c)(d)$ and MT-BCS-Jmn reconstructed object $(e)(f)(g)$ for Noiseless case $(b)(e)$, $SNR = 10$ [dB] $(c)(f)$ and $SNR = 5$ [dB] $(d)(g)$.

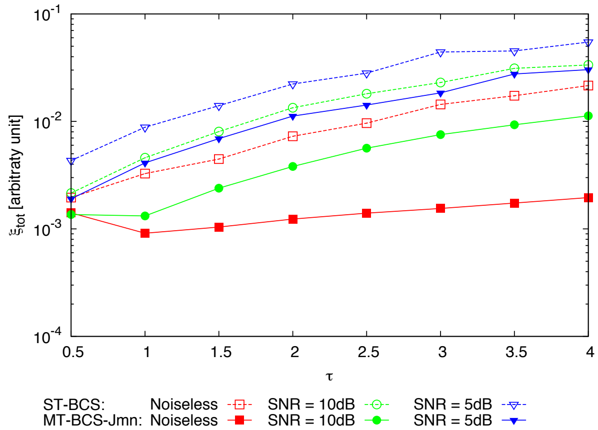

(a)

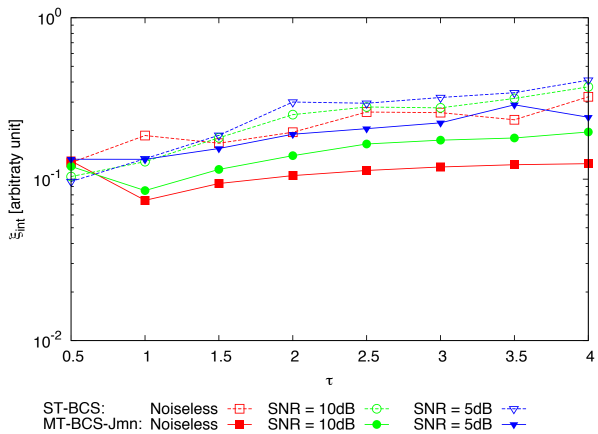

(b)

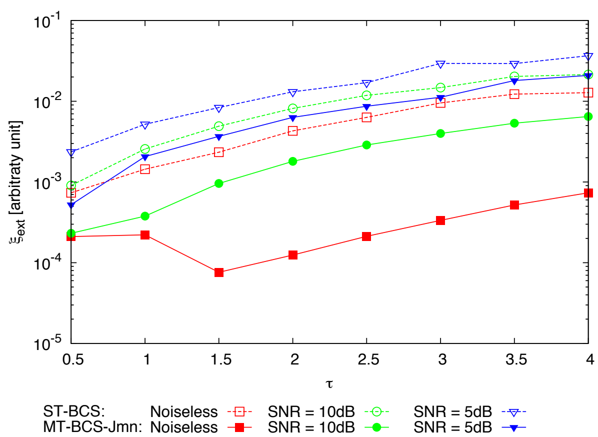

(c)

Figure 18. Behaviour of error figures as a function of ε_r, for different SNR values: (a) total error ξ_{tot}, (b) internal error ξ_{int}, (c) external error ξ_{ext}.

3.4 TEST CASE: Two Square Cylinders $L = 0.33\lambda$

Goal: show the performances of BCS when dealing with a sparse scatterer

- Number of Views: V
- Number of Measurements: M
- Number of Cells for the Inversion: N
- Number of Cells for the Direct solver: D
- Side of the investigation domain: L

Test Case Description

Direct solver:

- Square domain divided in $\sqrt{D} \times \sqrt{D}$ cells
- Domain side: $L = 3\lambda$
- $D = 1296$ (discretization for the direct solver: $< \lambda/10$)

Investigation domain:

- Square domain divided in $\sqrt{N} \times \sqrt{N}$ cells
- $L = 3\lambda$
- $2ka = 2 \times \frac{2\pi}{\lambda} \times \frac{L\sqrt{2}}{2} = 6\pi\sqrt{2} = 26.65$
- $\#DOF = \frac{(2ka)^2}{2} = \frac{(2\times\frac{2\pi}{\lambda}\times\frac{L\sqrt{2}}{2})^2}{2} = 4\pi^2\left(\frac{L}{\lambda}\right)^2 = 4\pi^2 \times 9 \approx 355.3$
- N scelto in modo da essere vicino a $\#DOF$: $N = 324$ (18×18)

Measurement domain:

- Measurement points taken on a circle of radius $\rho = 3\lambda$
- Full-aspect measurements
- $M \approx 2ka \rightarrow M = 27$

Sources:

- Plane waves
- $V \approx 2ka \rightarrow V = 27$
- Amplitude $A = 1$
- Frequency: 300 MHz ($\lambda = 1$)

Object:

- Two square cylinders of side $\frac{\lambda}{3} = 0.3333$
- $\varepsilon_r \in \{1.5, 2.0, 2.5, 3.0, 3.5, 4.0, 4.5, 5.0\}$
- $\sigma = 0$ [S/m]

MT-BCS-Jmn parameters:

- Gamma prior on noise variance parameter: $a = 5 \times 10^0$
- Gamma prior on noise variance parameter: $b = 8 \times 10^{-2}$
- Convergenze parameter: $\tau = 1.0 \times 10^{-8}$

RESULTS: Two Square Cylinders $L = 0.33\lambda$

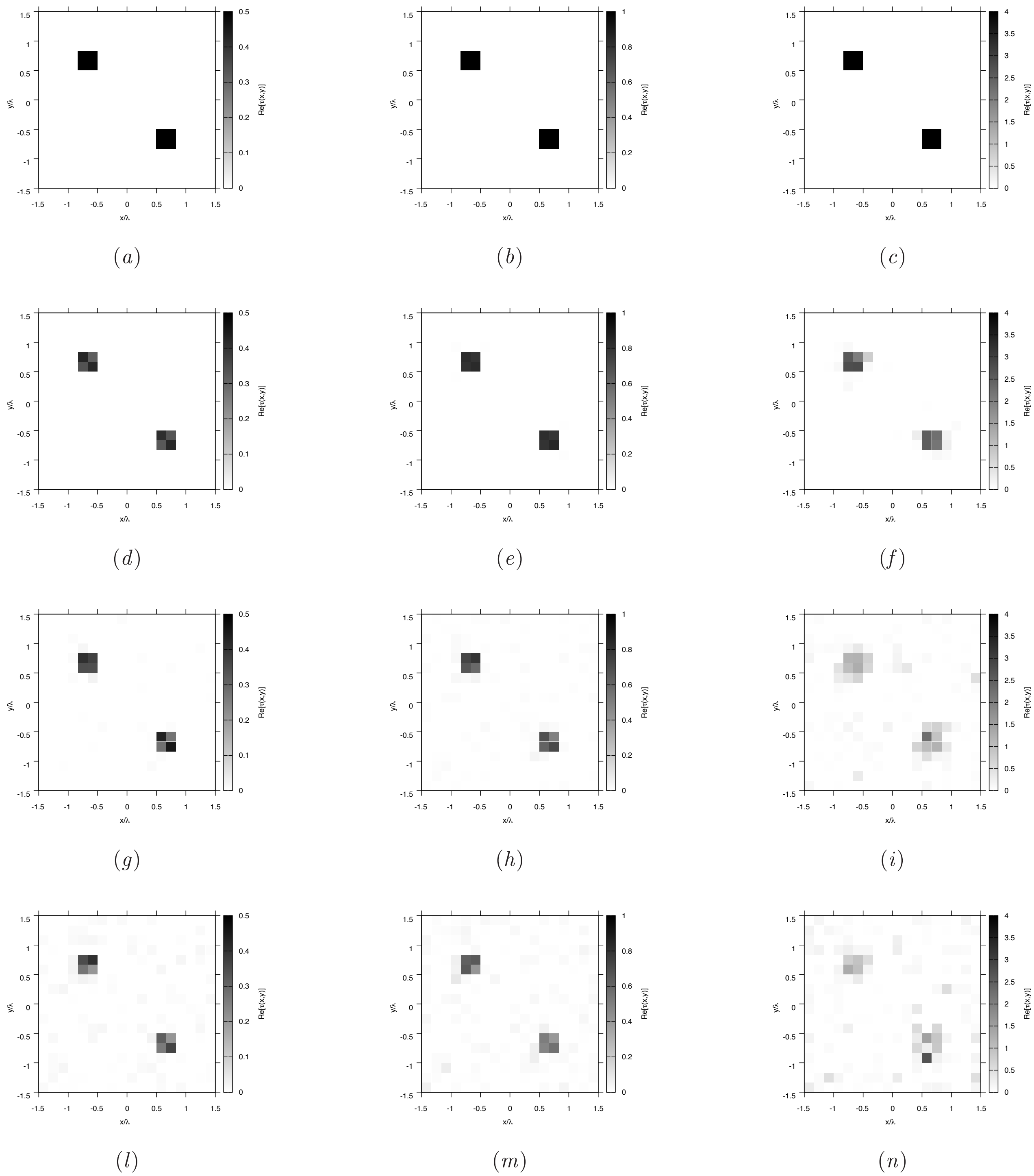

Figure 19. Actual object $(a)(b)(c)$ and MT-BCS-Jmn reconstructed object with $\varepsilon_r = 1.5$ $(d)(g)(l)$, $\varepsilon_r = 2.0$ $(e)(h)(m)$, and $\varepsilon_r = 5.0$ $(f)(i)(n)$, for Noiseless case $(d)(e)(f)$, $SNR = 10$ [dB] $(g)(h)(i)$ and $SNR = 5$ [dB] $(l)(m)(n)$.

RESULTS: Two Square Cylinders $L = 0.33\lambda$ - Reconstructions - Comparison ST-BCS/MT-BCS - $\varepsilon_r = 2.0$

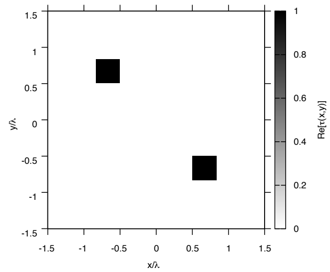

(a)

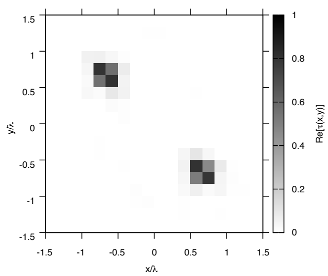

(b)

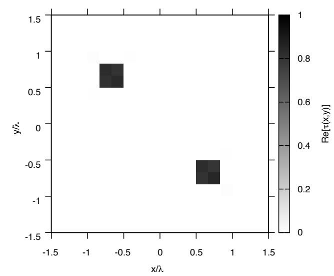

(e)

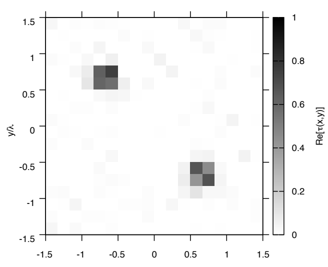

(c)

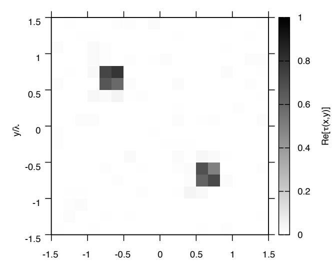

(f)

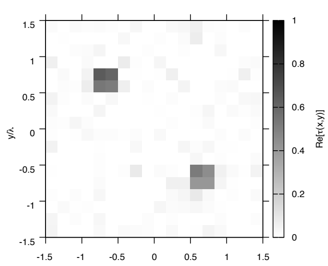

(d)

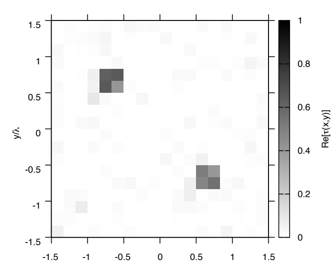

(g)

Figure 20. Actual object (a), ST-BCS reconstructed object $(b)(c)(d)$ and MT-BCS-Jmn reconstructed object $(e)(f)(g)$ for Noiseless case $(b)(e)$, $SNR = 10$ [dB] $(c)(f)$ and $SNR = 5$ [dB] $(d)(g)$.

RESULTS: Two Square Cylinders $L = 0.33\lambda$ - Error Figures - Comparison ST-BCS/MT-BCS

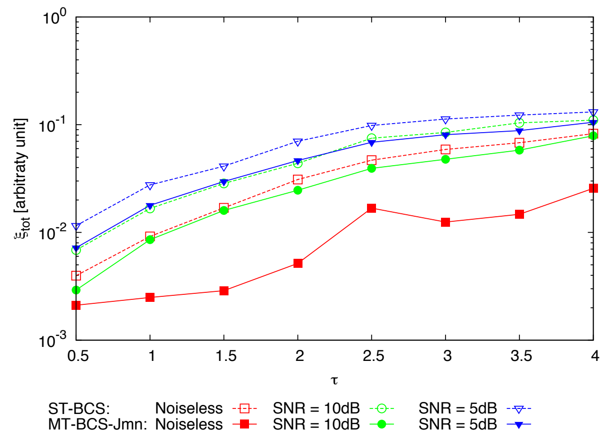

(a)

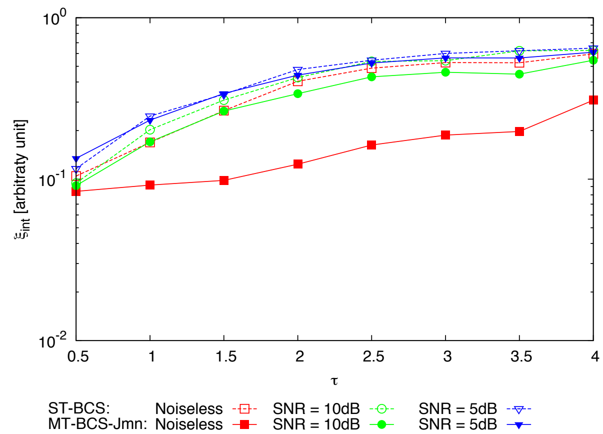

(b)

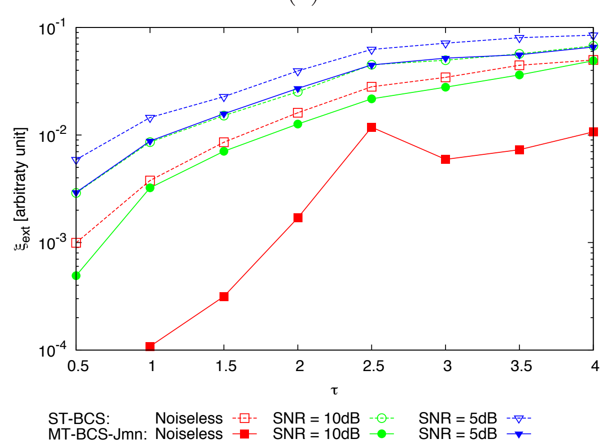

(c)

Figure 21. Behaviour of error figures as a function of ε_r, for different SNR values: (a) total error ξ_{tot}, (b) internal error ξ_{int}, (c) external error ξ_{ext}.

3.5 TEST CASE: Two L-shaped Cylinders

Goal: show the performances of BCS when dealing with a sparse scatterer

- Number of Views: V
- Number of Measurements: M
- Number of Cells for the Inversion: N
- Number of Cells for the Direct solver: D
- Side of the investigation domain: L

Test Case Description

Direct solver:

- Square domain divided in $\sqrt{D} \times \sqrt{D}$ cells
- Domain side: $L = 3\lambda$
- $D = 1296$ (discretization for the direct solver: $< \lambda/10$)

Investigation domain:

- Square domain divided in $\sqrt{N} \times \sqrt{N}$ cells
- $L = 3\lambda$
- $2ka = 2 \times \frac{2\pi}{\lambda} \times \frac{L\sqrt{2}}{2} = 6\pi\sqrt{2} = 26.65$
- $\#DOF = \frac{(2ka)^2}{2} = \frac{(2\times\frac{2\pi}{\lambda}\times\frac{L\sqrt{2}}{2})^2}{2} = 4\pi^2\left(\frac{L}{\lambda}\right)^2 = 4\pi^2 \times 9 \approx 355.3$
- N scelto in modo da essere vicino a $\#DOF$: $N = 324$ (18×18)

Measurement domain:

- Measurement points taken on a circle of radius $\rho = 3\lambda$
- Full-aspect measurements
- $M \approx 2ka \rightarrow M = 27$

Sources:

- Plane waves
- $V \approx 2ka \rightarrow V = 27$
- Amplitude $A = 1$
- Frequency: 300 MHz ($\lambda = 1$)

Object:

- Two L-shaped cylinders
- $\varepsilon_r \in \{1.5, 2.0, 2.5, 3.0, 3.5, 4.0, 4.5, 5.0\}$
- $\sigma = 0$ [S/m]

MT-BCS-Jmn parameters:

- Gamma prior on noise variance parameter: $a = 5 \times 10^0$
- Gamma prior on noise variance parameter: $b = 8 \times 10^{-2}$
- Convergenze parameter: $\tau = 1.0 \times 10^{-8}$

RESULTS: Two L-Shaped Cylinders

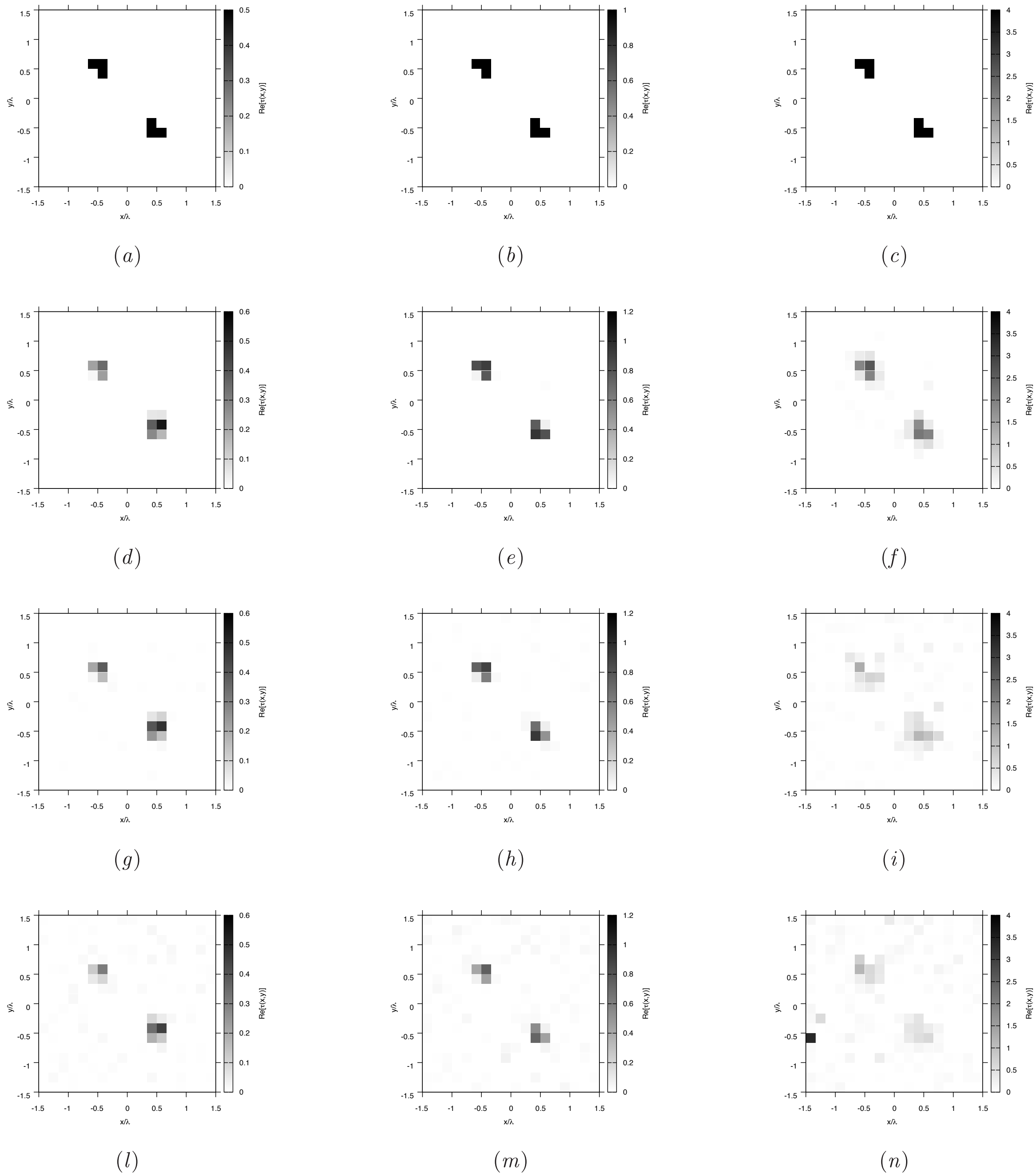

Figure 22. Actual object $(a)(b)(c)$ and MT-BCS-Jmn reconstructed object with $\varepsilon_r = 1.5$ $(d)(g)(l)$, $\varepsilon_r = 2.0$ $(e)(h)(m)$, and $\varepsilon_r = 5.0$ $(f)(i)(n)$, for Noiseless case $(d)(e)(f)$, $SNR = 10$ [dB] $(g)(h)(i)$ and $SNR = 5$ [dB] $(l)(m)(n)$.

RESULTS: Two L-Shaped Cylinders - Reconstructions - Comparison ST-BCS/MT-BCS - $\varepsilon_r = 2.0$

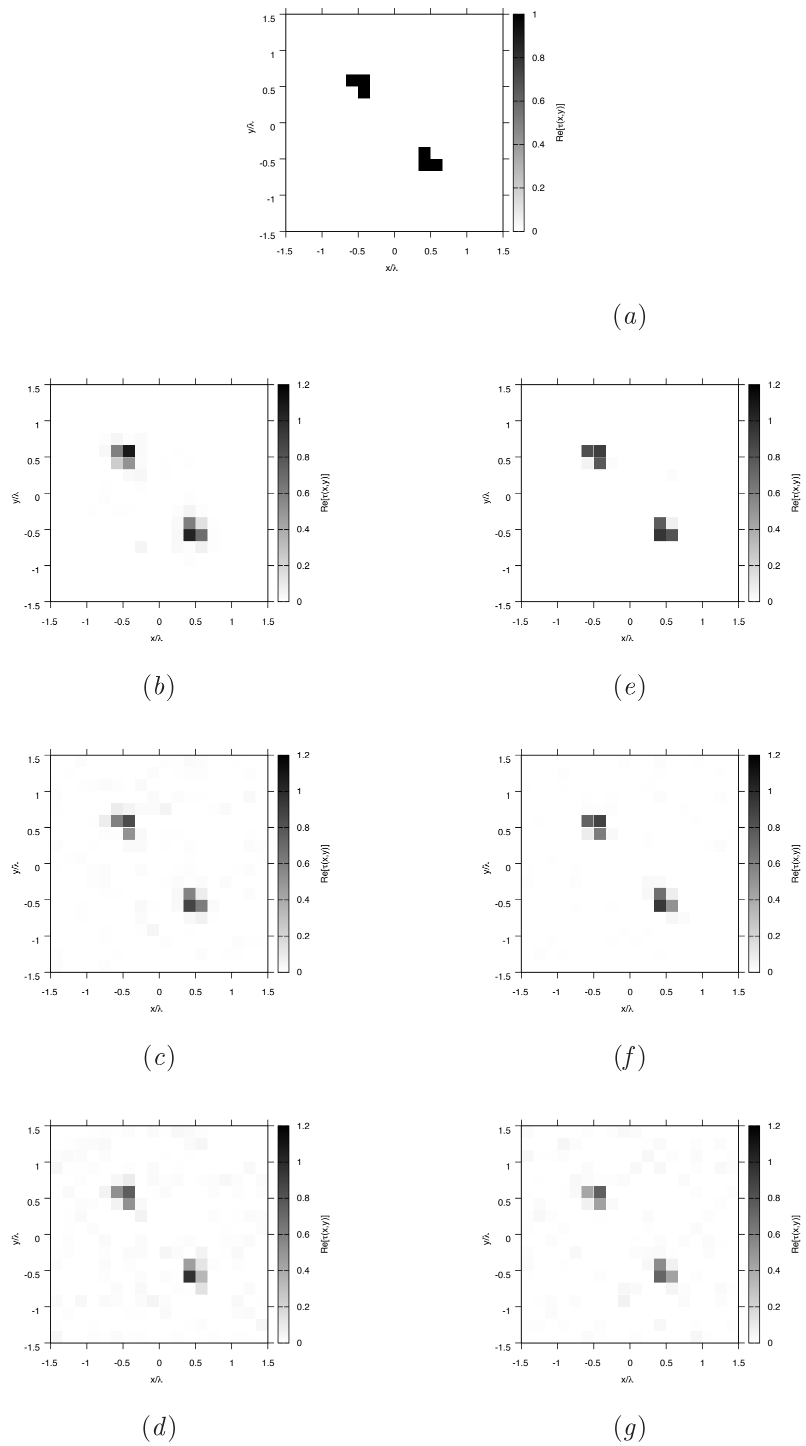

Figure 23. Actual object (a), ST-BCS reconstructed object $(b)(c)(d)$ and MT-BCS-Jmn reconstructed object $(e)(f)(g)$ for Noiseless case $(b)(e)$, $SNR = 10$ [dB] $(c)(f)$ and $SNR = 5$ [dB] $(d)(g)$.

RESULTS: Two L-Shaped Cylinders - Error Figures - Comparison ST-BCS/MT-BCS

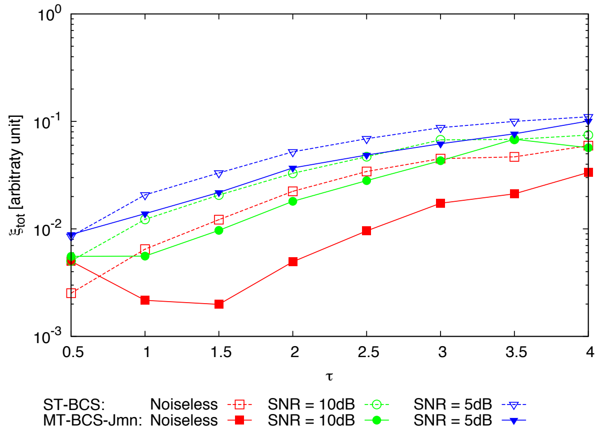

(a)

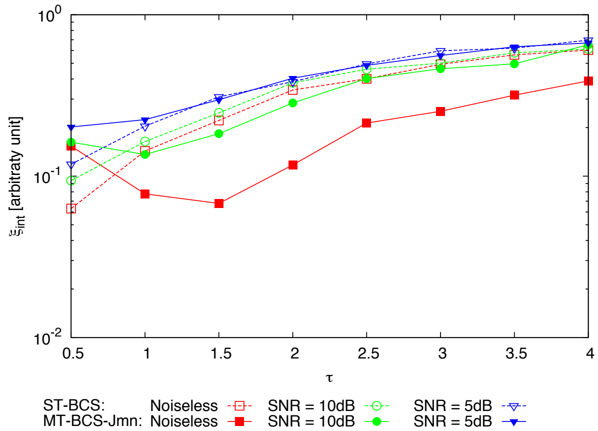

(b)

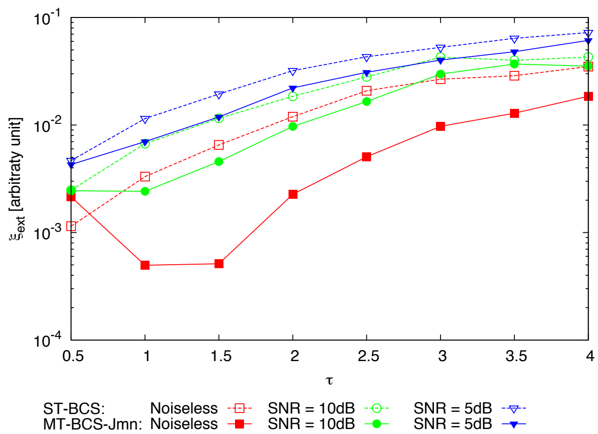

(c)

Figure 24. Behaviour of error figures as a function of ε_r, for different SNR values: (a) total error ξ_{tot}, (b) internal error ξ_{int}, (c) external error ξ_{ext}.

3.6 TEST CASE: Big L-shaped Cylinder

Goal: show the performances of BCS when dealing with a sparse scatterer

- Number of Views: V
- Number of Measurements: M
- Number of Cells for the Inversion: N
- Number of Cells for the Direct solver: D
- Side of the investigation domain: L

Test Case Description

Direct solver:

- Square domain divided in $\sqrt{D} \times \sqrt{D}$ cells
- Domain side: $L = 3\lambda$
- $D = 1296$ (discretization for the direct solver: $< \lambda/10$)

Investigation domain:

- Square domain divided in $\sqrt{N} \times \sqrt{N}$ cells
- $L = 3\lambda$
- $2ka = 2 \times \frac{2\pi}{\lambda} \times \frac{L\sqrt{2}}{2} = 6\pi\sqrt{2} = 26.65$
- $\#DOF = \frac{(2ka)^2}{2} = \frac{(2\times\frac{2\pi}{\lambda}\times\frac{L\sqrt{2}}{2})^2}{2} = 4\pi^2\left(\frac{L}{\lambda}\right)^2 = 4\pi^2 \times 9 \approx 355.3$
- N scelto in modo da essere vicino a $\#DOF$: $N = 324$ (18×18)

Measurement domain:

- Measurement points taken on a circle of radius $\rho = 3\lambda$
- Full-aspect measurements
- $M \approx 2ka \rightarrow M = 27$

Sources:

- Plane waves
- $V \approx 2ka \rightarrow V = 27$
- Amplitude $A = 1$
- Frequency: 300 MHz ($\lambda = 1$)

Object:

- Big L-shaped cylinder
- $\varepsilon_r \in \{1.5, 2.0, 2.5, 3.0, 3.5, 4.0, 4.5, 5.0\}$
- $\sigma = 0$ [S/m]

MT-BCS-Jmn parameters:

- Gamma prior on noise variance parameter: $a = 5 \times 10^0$
- Gamma prior on noise variance parameter: $b = 8 \times 10^{-2}$
- Convergenze parameter: $\tau = 1.0 \times 10^{-8}$

RESULTS: Big L-Shaped Cylinder

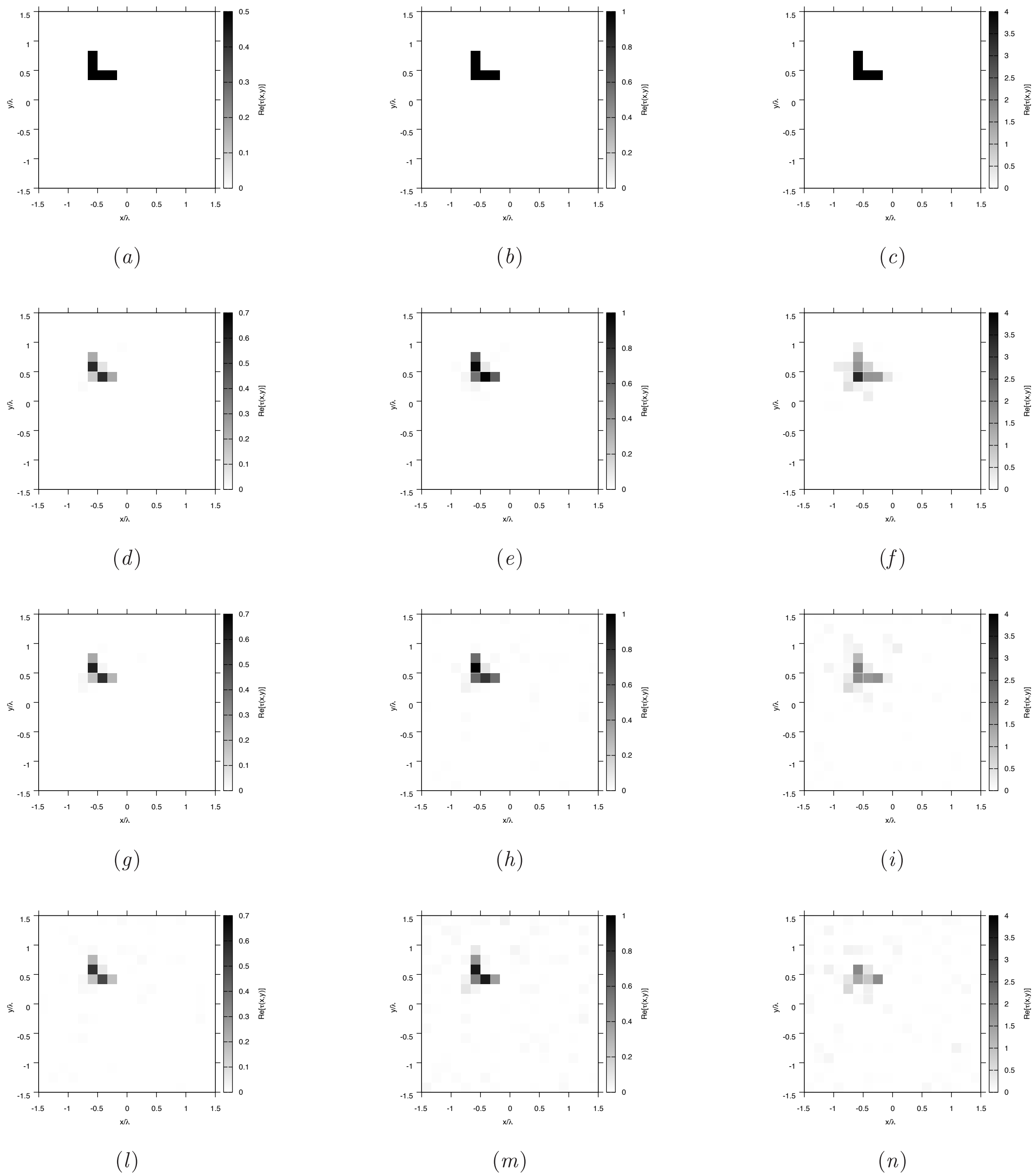

Figure 25. Actual object $(a)(b)(c)$ and MT-BCS-Jmn reconstructed object with $\varepsilon_r = 1.5$ $(d)(g)(l)$, $\varepsilon_r = 2.0$ $(e)(h)(m)$, and $\varepsilon_r = 5.0$ $(f)(i)(n)$, for Noiseless case $(d)(e)(f)$, $SNR = 10$ [dB] $(g)(h)(i)$ and $SNR = 5$ [dB] $(l)(m)(n)$.

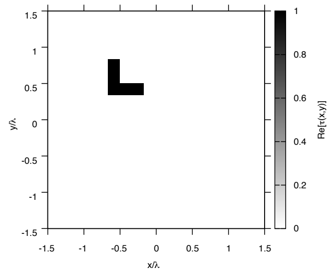

(a)

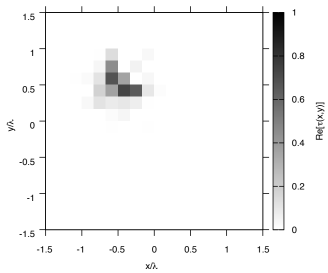

(b)

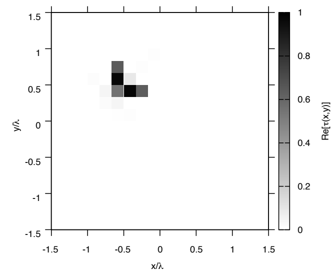

(e)

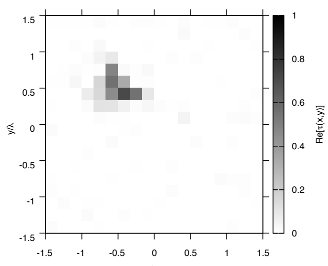

(c)

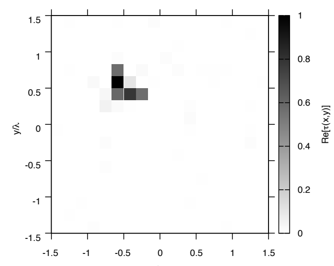

(f)

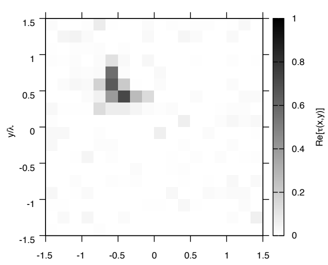

(d)

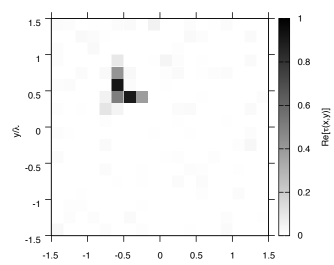

(g)

Figure 26. Actual object (a), ST-BCS reconstructed object $(b)(c)(d)$ and MT-BCS-Jmn reconstructed object $(e)(f)(g)$ for Noiseless case $(b)(e)$, $SNR = 10$ [dB] $(c)(f)$ and $SNR = 5$ [dB] $(d)(g)$.

RESULTS: Big L-Shaped Cylinder - Error Figures - Comparison ST-BCS/MT-BCS

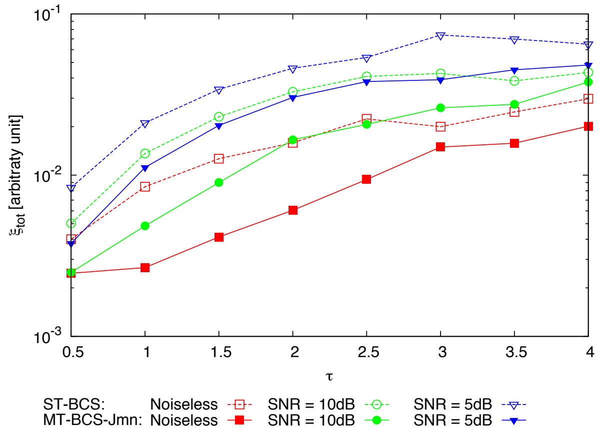

(a)

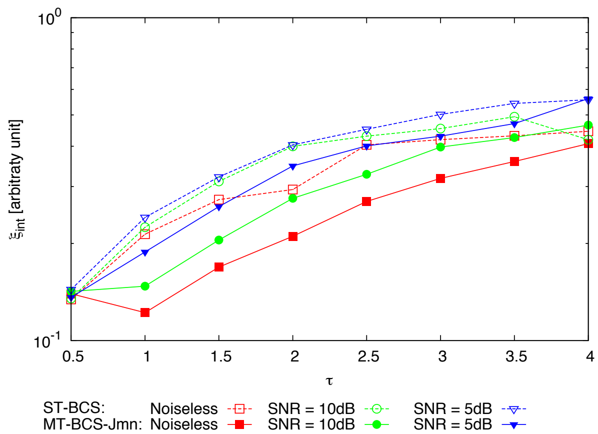

(b)

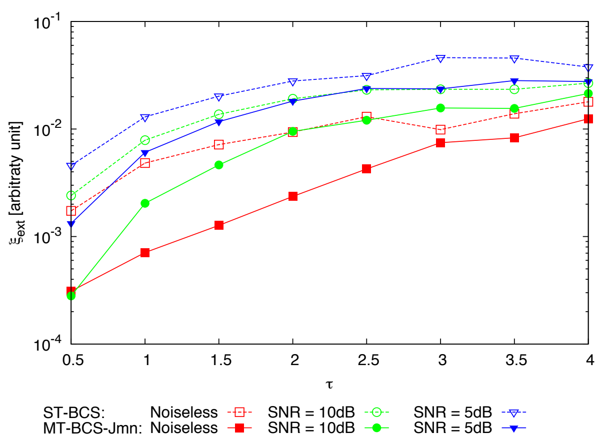

(c)

Figure 27. Behaviour of error figures as a function of ε_r, for different SNR values: (a) total error ξ_{tot}, (b) internal error ξ_{int}, (c) external error ξ_{ext}.

3.7 TEST CASE: Big T-shaped Cylinder

Goal: show the performances of BCS when dealing with a sparse scatterer

- Number of Views: V
- Number of Measurements: M
- Number of Cells for the Inversion: N
- Number of Cells for the Direct solver: D
- Side of the investigation domain: L

Test Case Description

Direct solver:

- Square domain divided in $\sqrt{D} \times \sqrt{D}$ cells
- Domain side: $L = 3\lambda$
- $D = 1296$ (discretization for the direct solver: $< \lambda/10$)

Investigation domain:

- Square domain divided in $\sqrt{N} \times \sqrt{N}$ cells
- $L = 3\lambda$
- $2ka = 2 \times \frac{2\pi}{\lambda} \times \frac{L\sqrt{2}}{2} = 6\pi\sqrt{2} = 26.65$
- $\#DOF = \frac{(2ka)^2}{2} = \frac{(2\times\frac{2\pi}{\lambda}\times\frac{L\sqrt{2}}{2})^2}{2} = 4\pi^2\left(\frac{L}{\lambda}\right)^2 = 4\pi^2 \times 9 \approx 355.3$
- N scelto in modo da essere vicino a $\#DOF$: $N = 324$ (18×18)

Measurement domain:

- Measurement points taken on a circle of radius $\rho = 3\lambda$
- Full-aspect measurements
- $M \approx 2ka \rightarrow M = 27$

Sources:

- Plane waves
- $V \approx 2ka \rightarrow V = 27$
- Amplitude $A = 1$
- Frequency: 300 MHz ($\lambda = 1$)

Object:

- Big T-shaped cylinder
- $\varepsilon_r \in \{1.5, 2.0, 2.5, 3.0, 3.5, 4.0, 4.5, 5.0\}$
- $\sigma = 0$ [S/m]

MT-BCS-Jmn parameters:

- Gamma prior on noise variance parameter: $a = 5 \times 10^0$
- Gamma prior on noise variance parameter: $b = 8 \times 10^{-2}$
- Convergenze parameter: $\tau = 1.0 \times 10^{-8}$

RESULTS: Big T-Shaped Cylinder

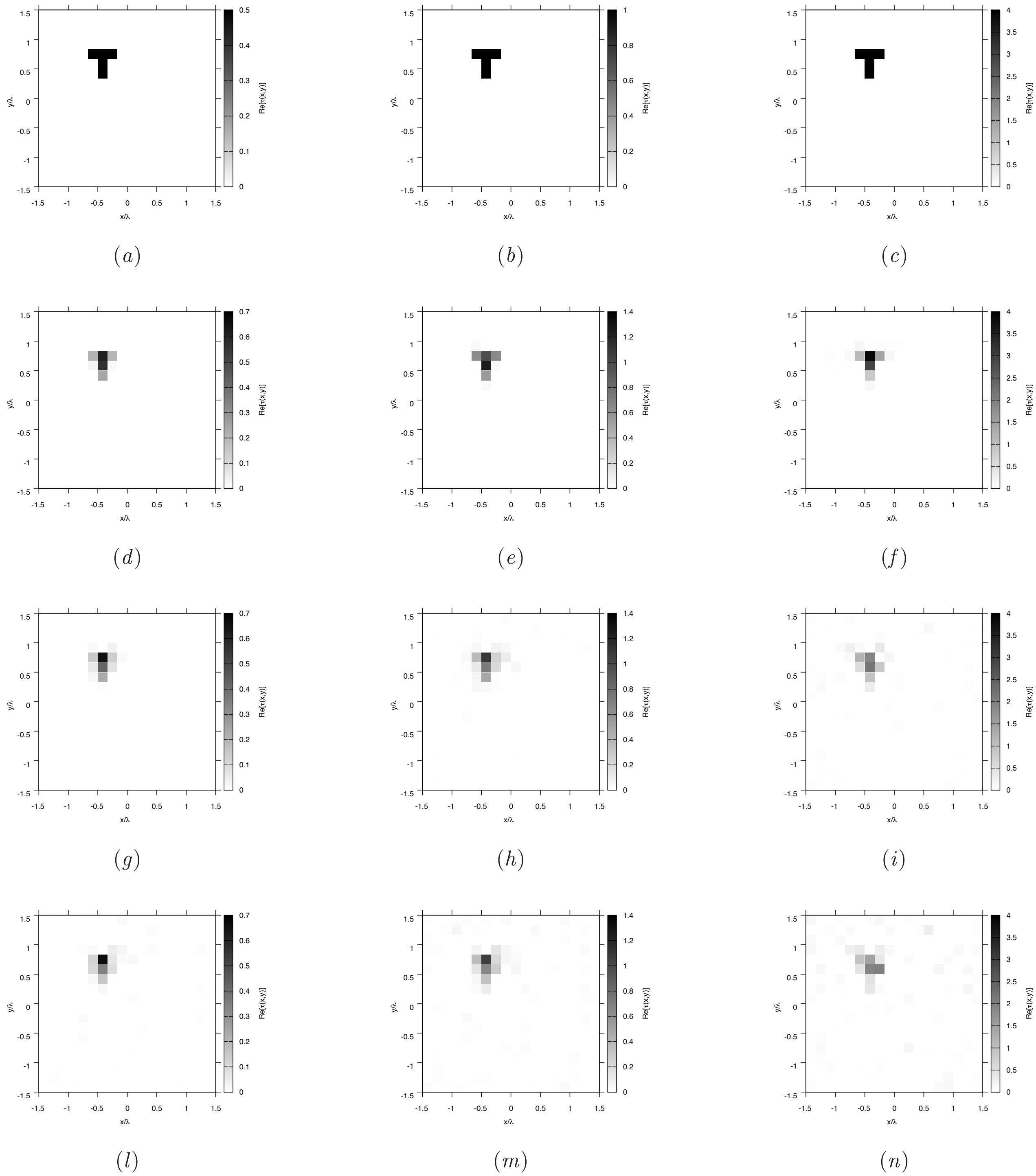

Figure 28. Actual object $(a)(b)(c)$ and MT-BCS-Jmn reconstructed object with $\varepsilon_r = 1.5$ $(d)(g)(l)$, $\varepsilon_r = 2.0$ $(e)(h)(m)$, and $\varepsilon_r = 5.0$ $(f)(i)(n)$, for Noiseless case $(d)(e)(f)$, $SNR = 10$ [dB] $(g)(h)(i)$ and $SNR = 5$ [dB] $(l)(m)(n)$.

RESULTS: Big T-Shaped Cylinder - Reconstructions - Comparison ST-BCS/MT-BCS - $\varepsilon_r = 2.0$

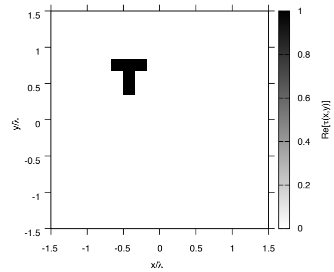

(a)

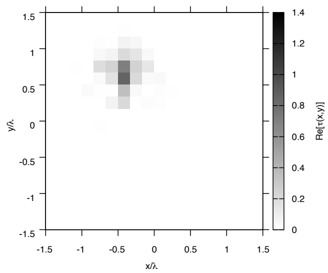

(b)

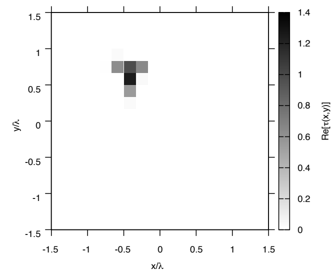

(e)

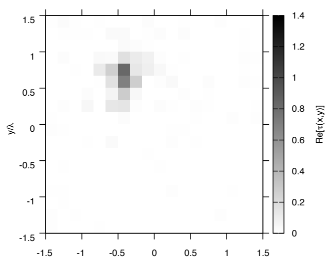

(c)

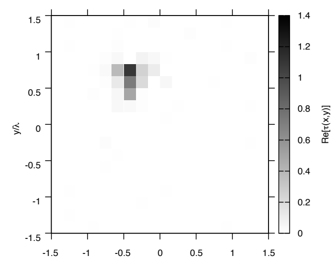

(f)

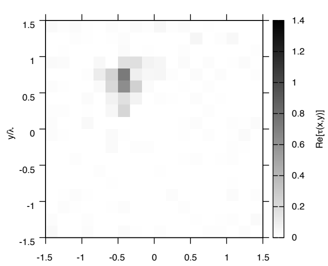

(d)

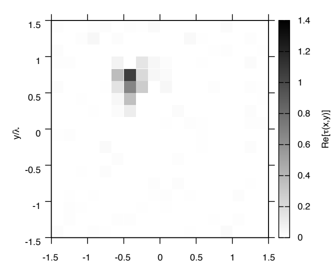

(g)

Figure 29. Actual object (a), ST-BCS reconstructed object $(b)(c)(d)$ and MT-BCS-Jmn reconstructed object $(e)(f)(g)$ for Noiseless case $(b)(e)$, $SNR = 10$ [dB] $(c)(f)$ and $SNR = 5$ [dB] $(d)(g)$.

RESULTS: Big T-Shaped Cylinder - Error Figures - Comparison ST-BCS/MT-BCS

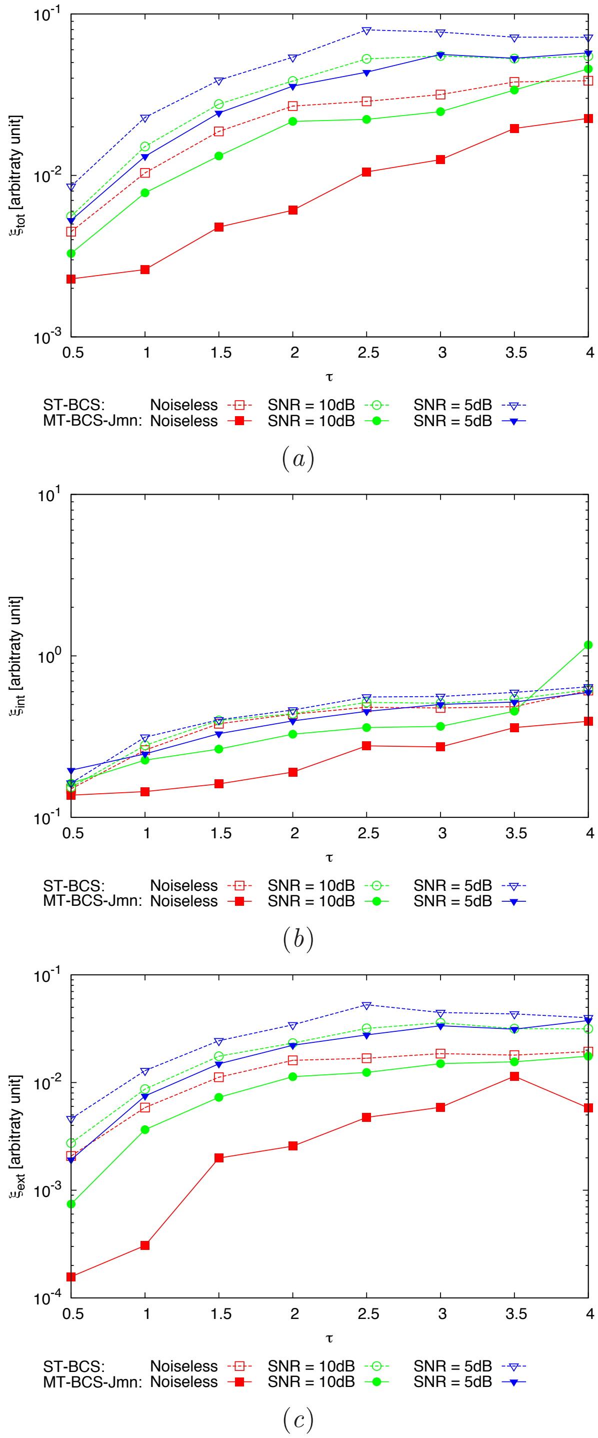

Figure 30. Behaviour of error figures as a function of ε_r, for different SNR values: (a) total error ξ_{tot}, (b) internal error ξ_{int}, (c) external error ξ_{ext}.

References

[1] G. Oliveri, N. Anselmi, and A. Massa, "Compressive sensing imaging of non-sparse 2D scatterers by a total-variation approach within the Born approximation," IEEE Trans. Antennas Propag., vol. 62, no. 10, pp. 5157-5170, Oct. 2014.

[2] L. Poli, G. Oliveri, and A. Massa, "Imaging sparse metallic cylinders through a Local Shape Function Bayesian Compressive Sensing approach," Journal of Optical Society of America A, vol. 30, no. 6, pp. 1261-1272, 2013.

[3] F. Viani, L. Poli, G. Oliveri, F. Robol, and A. Massa, "Sparse scatterers imaging through approximated multitask compressive sensing strategies," Microwave Opt. Technol. Lett., vol. 55, no. 7, pp. 1553-1558, Jul. 2013.

[4] L. Poli, G. Oliveri, P. Rocca, and A. Massa, "Bayesian compressive sensing approaches for the reconstruction of two-dimensional sparse scatterers under TE illumination," IEEE Trans. Geosci. Remote Sensing, vol. 51, no. 5, pp. 2920-2936, May. 2013.

[5] L. Poli, G. Oliveri, and A. Massa, "Microwave imaging within the first-order Born approximation by means of the contrast-field Bayesian compressive sensing," IEEE Trans. Antennas Propag., vol. 60, no. 6, pp. 2865-2879, Jun. 2012.

[6] G. Oliveri, P. Rocca, and A. Massa, "A bayesian compressive sampling-based inversion for imaging sparse scatterers," IEEE Trans. Geosci. Remote Sensing, vol. 49, no. 10, pp. 3993-4006, Oct. 2011.

[7] G. Oliveri, L. Poli, P. Rocca, and A. Massa, "Bayesian compressive optical imaging within the Rytov approximation," Optics Letters, vol. 37, no. 10, pp. 1760-1762, 2012.

[8] L. Poli, G. Oliveri, F. Viani, and A. Massa, "MT-BCS-based microwave imaging approach through minimum-norm current expansion," IEEE Trans. Antennas Propag., vol. 61, no. 9, pp. 4722-4732, Sept. 2013.

[9] G. Oliveri and A. Massa, "Bayesian compressive sampling for pattern synthesis with maximally sparse non-uniform linear arrays," IEEE Trans. Antennas Propag., vol. 59, no. 2, pp. 467-481, Feb. 2011.

[10] G. Oliveri, M. Carlin, and A. Massa, "Complex-weight sparse linear array synthesis by Bayesian Compressive Sampling," IEEE Trans. Antennas Propag., vol. 60, no. 5, pp. 2309-2326, May 2012.

[11] G. Oliveri, P. Rocca, and A. Massa, "Reliable Diagnosis of Large Linear Arrays - A Bayesian Compressive Sensing Approach," IEEE Trans. Antennas Propag., vol. 60, no. 10, pp. 4627-4636, Oct. 2012.

[12] F. Viani, G. Oliveri, and A. Massa, "Compressive sensing pattern matching techniques for synthesizing planar sparse arrays," IEEE Trans. Antennas Propag., vol. 61, no. 9, pp. 4577-4587, Sept. 2013.

[13] G. Oliveri, E. T. Bekele, F. Robol, and A. Massa, "Sparsening conformal arrays through a versatile BCS-based method," IEEE Trans. Antennas Propag., vol. 62, no. 4, pp. 1681-1689, Apr. 2014.